Fermi National Accelerator Laboratory

FERMILAB-Pub-94/367

Mass and Decay Time Resolution for Beauty Physics at Hadron Colliders

Christopher J. Kennedy, Robert F. Harr and Paul E. Karchin

Fermi National Accelerator Laboratory
P.O. Box 500, Batavia, Illinois 60510

Physics Department, Yale University
New Haven, Connecticut 06520-8121

October 1994

Submitted to *Physical Review D*

Operated by Universities Research Association Inc. under Contract No. DE-AC02-76CHO3000 with the United States Department of Energy

Disclaimer

Mass and Decay Time Resolution for Beauty Physics at Hadron Colliders

Christopher J. Kennedy, Robert F. Harr, Paul E. Karchin

Physics Department, Yale University

New Haven, Connecticut 06520-8121

(Work carried out as part of a Fermilab Expression of Interest.)

Abstract

The large cross section for beauty production in hadron interactions at the highest available energies leads to unique opportunities to measure precisely CP violation and mixing in B-decays. We assess the ability of two representative collider detector configurations, central and forward, to measure decays of interest. We study the decays $B_d^0 \to \pi^+\pi^-$ and $B_d^0 \to J/\psi K_s$, which are sensitive to CP violation, and $B_s^0 \to D_s^-\pi^+\pi^+\pi^-$, which is sensitive to the mixing parameter, x_s. We investigate the mass and decay time resolution for B-production at three accelerator facilities: RHIC, the Tevatron and LHC.

Particles from Monte Carlo generated B-decays are traced through a detailed detector model to obtain track error matrices. These are combined to calculate the mass and decay time resolutions. This technique gives accurate estimates of resolutions without a time consuming hit level simulation, so it is well suited for design studies. To demonstrate further the utility of this technique, we examine the effects of varying three important parameters of a silicon vertex detector: inner radius, spatial resolution, and stereo angle.

I. INTRODUCTION

Understanding CP violation in beauty decays is an important goal in particle physics [1]. To map out fully CP violation, the angles of the unitarity triangle (α, β, and γ) must be precisely measured. The angles α and β can be determined by measuring the B^0- $\overline{B}^0$ decay rate asymmetry in $B_d^0 \to \pi^+\pi^-$ and $B_d^0 \to J/\psi\, K_s$, respectively. These two decays are the most favorable because of an unambiguous theoretical interpretation and simple experimental signature. Several prospects for measuring γ involve decays of B_s [2,3]. B_s measurements are difficult due to the large value of x_s, the mixing parameter of the B_s meson. It is of interest to measure x_s since it is a fundamental parameter of the standard model and is related to $|V_{ts}|$. We consider the measurement of x_s via $B_s^0 \to D_s^- \pi^+\pi^+\pi^-$ because of its expected high branching ratio and all charged final state.

The large cross section for beauty production in hadron interactions leads to unique opportunities to perform high statistics B decay measurements. This has prompted proposals for B-physics experiments at RHIC, the Tevatron, LHC, and SSC.

We report the results of studies, done in part for an expression of interest at Fermilab [4], on the expected performance of detectors at these high energy hadron accelerators. These studies examine the effect of detector configuration on mass and decay time resolution, and acceptance. Good resolution is needed to eliminate backgrounds, good decay time resolution is necessary to measure B-mixing, and good acceptance is necessary for any high statistics study. We consider two different geometries, forward and central, representative of the large number of potential detector configurations. We employ detailed models of vertexing and tracking detectors, which take into account spatial resolution and scattering material. We investigate the effects of varying important vertex detector parameters: inner radius, spatial resolution, and stereo angle.

We use a Monte Carlo simulation to generate B-events and then analytically calculate the track error matrices for selected final state particles. The unperturbed particle trajectories are overlayed on the model of the vertex and tracking detectors. The trajectory, the detector

resolutions, and the effects of multiple Coulomb scattering are used to calculate the error matrix for each track. The error matrix contains the correlated errors in position, direction and momentum. The track error matrices are combined to calculate the position and mass resolution of each decay. This technique gives accurate mass and decay time resolution without a time consuming hit level simulation. The low computing load allows a large number of detector parameters to be analyzed quickly.

A detector parameter file defines the detector layers, such as silicon microstrips and drift cells, and scattering material, such as beam pipes, support structures and windows. The parameters include shape, position, orientation, thickness, material, measurement resolution and measurement direction.

II. METHOD

The first step is to generate B-events using PYTHIA 5.6 and JETSET 7.3 [5]. For each decay mode and center of mass energy, 10,000 events are generated and saved in an interim file. This event sample is reused for each detector configuration. Acceptance of a track is based on its traversing a minimum number of detector planes, discussed in more detail later. For each accepted charged particle, the error matrix is determined using the Kalman filter technique [6]. The implementation of this technique for the geometries considered is described in detail in Ref. [7].

In the next step, the track error matrices of selected final state particles are combined to calculate the mass resolution and the secondary vertex error matrix from a constrained vertex fit [7]. The primary vertex error matrix is calculated utilizing all accepted charged tracks from the primary vertex. The distance of separation between the primary and secondary vertex is designated L. The primary and secondary vertex error matrices are used to determine the error on the separation between the vertices, δL, and the significance of separation, $L/\delta L$. Along with the particle's mass and momentum, δL is used to determine the error on the proper time of the decay, $\delta\tau$.

The decay mode primarily studied is $B_d^0 \to J/\psi\, K_s$ where $J/\psi \to \mu^+\mu^-$ and $K_s \to \pi^+\pi^-$. This decay is representative of a broader class of B-decays that are likely to be of interest, for instance, $B_s^0 \to J/\psi\, \phi$. Both decays have a multiplicity of four which is typical for B-decays. Results from $B_d^0 \to J/\psi\, K_s$ are applicable to other modes with comparable multiplicity. Since this mode is not "self tagging", a decay product from the other B hadron must be used to identify the particle/antiparticle nature of the B_d^0 at production. In this analysis an electron or muon is used as the "tag". Previous studies indicate that a muon or dimuon trigger significantly reduces minimum bias background while maintaining a high signal efficiency [8]. CDF has observed this decay [9], evidence that it can be triggered and reconstructed in a hadronic environment.

A. Beauty-Production

In the forseeable future, there will be 3 hadron colliders suitable for an hadronic B-physics experiment: RHIC[1], the Tevatron, and LHC (see Table ??). The cross sections presented in the table are those predicted by Berger and Meng using next to leading order QCD [10]. As the energy of the machine increases, the B-production cross section increases, and the B-hadrons are produced over a greater range of pseudo-rapidity (η), as seen in Fig. 1. This broadening leads to significant differences in the fraction of accepted events in each detector. The slight differences in the transverse momentum spectra at different energies, predicted by PYTHIA, do not significantly affect the resolutions studied. Thus, while most of the results presented here are for the Tevatron energy, they are representative of all three energies.

---

[1]We consider only the $p\bar{p}$ running mode of RHIC for B-physics. Of course, experimenters must take into account that RHIC is primarily a heavy ion collider and the $p\bar{p}$ mode will account for only a fraction of the running.

B. Central Detector

The central detector model, shown schematically in Fig. 2, is based on the current CDF detector [11] and planned upgrades [12]. We base our model on the CDF detector because it is an existing device and, although it is designed as a general purpose, high p_T detector, it provides a good starting point for the design of a future dedicated beauty experiment with central geometry. Three subsystems are included in the model: the silicon vertex detector (SVX), the vertex time projection chamber (VTPC), and the central tracking chamber (CTC). The parameters of this model are summarized in Table ??. Each of the 4 SVX layers is a 300 μm thick double sided detector with strips oriented to measure in the beam and azimuthal directions (z and ϕ). We assume that, except for the silicon, there is negligible material in the tracking volume (electronics and support structure). The VTPC has 16 equally spaced layers. The scattering in each layer is equivalent to 0.75 cm of gas; other material within its 160 cm length is omitted. The CTC has 84 equally spaced layers, each modeled as having a resolution of 200 μm transverse to the sense wires. The sense wires are positioned along, or at a small stereo angle to, the z direction, as shown in Fig. 2. The scattering in each layer is equivalent to 1.2 cm of gas; again, wires have been omitted.

For a track to be "measured" it must traverse the 4 layers of the SVX, the 16 layers of the VTPC, and 30 of the 84 layers of the CTC and have a momentum of at least 0.5 GeV. Tracks that do not traverse a sufficient number of layers fall into two categories: those that exit the detector due to a large $|\eta|$, and those that curl up in the magnetic field due to a small transverse momentum. The solenoidal magnetic field has a strength of 1.5 T.

We make the simplifying assumption that the production vertex of each event is at the origin of the coordinates. The effect of an extended luminous region is a decrease in acceptance. For example, the acceptance is 18% smaller for a tagged $B_d^0 \to J/\psi\, K_s$ decay when the RMS length of the luminous region is 35 cm than when it is zero. There is no effect on the mass or vertex resolutions from extending the luminous region.

To check the error matrix calculations, we use the formulae of Gluckstern [13]. Gluckstern

derives formulae for some elements of the track error matrix, valid for a solenoidal detector in the high p_T limit, as discussed in Ref. [7]. We find that our results are in agreement with these formulae to better than 1%. To further check the accuracy of our method, we model the current CDF detector and compare our calculation of resolutions to results from CDF. In CDF's measurement of the average B lifetime using the decay $B \to J/\psi X \to \mu^+\mu^- X$ [14], they obtain an RMS width of $16\,\mathrm{MeV/c^2}$ on the reconstructed J/ψ mass peak, and a mean transverse vertex resolution of $\approx 60\,\mu\mathrm{m}$. Using a sample of $B_d^0 \to J/\psi\, K_s$ decays, we estimate the RMS width of the J/ψ mass peak to be $13\,\mathrm{MeV/c^2}$, and the mean transverse vertex resolution to be $63\,\mu\mathrm{m}$. The agreement between the mean transverse vertex resolution is quite good and the agreement between the widths of the mass peaks is good considering that our analysis does not take into account pattern recognition, detector efficiencies, and other experimental characteristics.

C. Forward Detector

We consider a forward detector for beauty physics at a hadron collider adapted from the successful charm fixed-target experiments. It consists of two parts: a fully modeled vertex detector, and a parameterized downstream magnetic spectrometer. The parameters of this detector are shown in Table ??. Although the collider environment allows for forward and backward spectrometers, we model only a single arm. The vertex detector (see Fig. 3) consists of 10 equally spaced planes of double sided silicon strip detectors. The acceptance of the downstream spectrometer is modeled by requiring $\eta > 1.5$. For a forward collider detector, the downstream spectrometer is similar to a fixed target spectrometer. Since the momentum resolution from fixed target magnetic spectrometers is well understood, we use a parameterization from the Fermilab E687 spectrometer [15]:

$$\frac{\sigma_p}{p} = 1.4\% \left(\frac{p}{100\,\mathrm{GeV/c}}\right) \sqrt{1 + \left(\frac{23\,\mathrm{GeV/c}}{\mathrm{p}}\right)^2}, \qquad (2.1)$$

which is representative of fixed target spectrometers. For a track to be "measured" it must have p > 0.5 GeV, and traverse at least three vertex detector planes.

As with the central detector, a single interaction point is used. For an extended luminous region, the vertex detector can be extended by adding additional planes with the same spacing. The extension of the vertex detector allows the acceptance to remain the same as for a point luminous region. The acceptance of the downstream spectrometer does not change, since its length is much larger than the luminous region at any of the accelerators we are studying.

In an alternate design, the vertex detector is placed inside the beam pipe, separated from the beams by a thin RF shield [16]. The main advantage of this design is that the silicon planes can be placed closer to the beams than if they were outside of the beampipe. We modeled a detector without a beampipe at the Tevatron energy and found that the mass and vertex resolutions are similar to our model with a beampipe. Therefore, the results from our model are applicable to both forward detector designs.

III. RESULTS

A. Acceptance

Acceptance is important since both decay asymmetry and mixing measurements require high statistics. Since the differential cross section broadens in η_B with increasing energy, the number of events accepted depends on energy. We examine $B_d^0 \rightarrow J/\psi\, K_s$, where $J/\psi \rightarrow \mu^+\mu^-$ and $K_s \rightarrow \pi^+\pi^-$. Since both mixing and decay asymmetry measurements require that the initial state of the B^0 is known, a tag is required. The tag that is used is an electron or muon from the $\overline{B}$. For the decay to be accepted, all 5 particles (the two muons, two pions, and the tag) must be accepted. The semi-leptonic branching ratio is assumed to be 21% and is included in the acceptance results shown in Table ??. The accepted fraction varies significantly at the different accelerators. At RHIC there is a 6 : 1 numerical

advantage for the central detector for $B_d^0 \to J/\psi\, K_s$. At the Tevatron, this advantage is reduced to 30%. At the LHC, the forward detector has a 30% advantage over the central detector. The acceptances of tagged $B_d^0 \to \pi^+\pi^-$ and $B_s^0 \to D_s^-\pi^+\pi^+\pi^-$ are also shown in Table ??. For these two decay modes, a similar trend is seen of increasing acceptance in the forward detector and decreasing acceptance in the central detector for increasing energy.

B. Proper Time Resolution and Significance of Separation for $B_d^0 \to \psi K_s$

Good proper time resolution is necessary for a variety of reasons. The precision of unitarity triangle measurements from decay asymmetries is enhanced if the time dependance of the asymmetries can be accurately measured. Also, decay time information is necessary for mixing measurements. Finally, non-B backgrounds can be reduced by requiring a minimum $L/\delta L$, a quantity which is approximately the same as $\tau/\delta\tau$.

The primary vertex resolution, δL_p, is determined from tracks that are in the acceptance of the detector. The error matrices from these tracks are calculated and combined in a constrained-vertex fit to determine the error matrix of the vertex. Projecting the vertex error on the direction of the decaying B yields δL_p.

The secondary vertex resolution, δL_s, is determined by performing a constrained vertex fit with the final state decay products originating at the B decay vertex. For $B_d^0 \to J/\psi\, K_s$, the two muons from the J/ψ decay determine the vertex. Again, δL_s is found by projecting the vertex error matrix along the direction of the decaying B.

We found that δL_p and δL_s of the central detector and δL_p of the forward detector do not depend on η_B, the η of the parent B. However, δL_s of the forward detector does depend on η_B, as discussed below. Additionally, we found that the distribution of δL_s for the central detector has a long tail and is not well characterized by the mean, $\langle \delta L_s \rangle$. However, the distributions of the forward detector are well characterized by their means. For these reasons, δL_p and δL_s are displayed differently for the forward and central detectors. Fig. 4 is for the central detector. The distributions of δL_p and δL_s are both characterized by a

peak and a tail. The peak of the distribution of δL_p is at a lower value than that of δL_s. Fig. 5 shows $\langle \delta L_p \rangle$ and $\langle \delta L_s \rangle$ versus η_B for the forward detector. $\langle \delta L_p \rangle$ is independent of η_B and is roughly the same as for the central detector, about 35 μm. $\langle \delta L_s \rangle$ quickly degrades with increasing η_B and ranges from 35 μm at $\eta_B = 2$ to greater than 140 μm at $\eta_B = 4$. This degradation with η_B is due to the correlated increase of the B momentum with η, which leads to a smaller opening angle.

The error on the separation of the vertices, δL, is the sum in quadrature of the individual errors, since they are uncorrelated. This calculation is dominated by δL_s in the central detector. This is also true in the forward detector except at small values of η_B where the primary and secondary vertex resolutions are similar.

Significance of separation, $L/\delta L$, is a useful figure of merit for comparing detectors. The mean, $\langle L/\delta L \rangle$, versus η_B is shown in Fig. 6 for both detectors. The forward detector has more favorable values of $\langle L/\delta L \rangle$ independent of η_B, due to a variety of reasons. The momentum increases with η_B, so the multiple scattering contribution is reduced. Also, due to the differences in geometry, the forward detector accepts decays with a higher average momentum for the same value of η_B. Additional differences are that the forward detector has a smaller radius and is oriented so that tracks at high η traverse less scattering material. Some of these effects will be discussed in more detail later.

The results presented above are for the Tevatron. We also studied δL and $L/\delta L$ for RHIC and LHC; the results are similar to those for the Tevatron. A minor difference is that the multiplicity of the primary vertex increases with energy. Therefore, the primary vertex resolution improves with energy. Since the secondary vertex resolution dominates, there is little difference in the total resolution.

C. Proper Time Resolution and Significance of Separation for $B_d^0 \to \pi^+\pi^-$ and $B_s^0 \to D_s^-\pi^+\pi^+\pi^-$

Since both good proper time resolution and acceptance are necessary for decay asymmetry and mixing measurements, we examine the distribution of proper time resolution, $\delta\tau$, of accepted events. We do not require a tag for these events. For the study of $B_s^0 \to D_s^-\pi^+\pi^+\pi^-$, we force $D_s^- \to \phi\pi^-$ and $\phi \to K^+K^-$. The error matrix for the D_s^- is calculated from those of its decay products and combined with those of the pions to calculate the error matrix of the B_s^0 vertex. In Figs. 7-9 we compare the distributions of $\delta\tau$ for $B_s^0 \to D_s^-\pi^+\pi^+\pi^-$ at the three colliders for the central and forward detectors. For all three colliders, $\delta\tau$ is better for the forward detector. However, at RHIC, the smaller accepted fraction negates the advantage of better resolution. Assuming a luminosity of $5 \times 10^{32}\text{cm}^{-2}\text{s}^{-1}$ and 10^6 seconds of running at RHIC, the forward detector would accept about 350 tagged $B_s^0 \to D_s^-\pi^+\pi^+\pi^-$ events per year and a central detector about 1600. Trigger, reconstruction, and tagging efficiencies would further reduce these numbers, making the forward detector option at RHIC less attractive in comparison. At the Tevatron, the better resolution comes at little cost in acceptance. At LHC, a forward detector presents an overwhelming advantage in resolution and has a better acceptance.

Comparing the proper time resolution of the central and forward detector, there is about a factor of 6 difference. To qualitatively understand this difference we tried to identify the principle factor determining the overall proper time resolution. Although the proper time resolution depends on η_B and the geometry of the decay, we find it is most highly correlated with the momentum of the B, P_B. The relationship between $\delta\tau$ and P_B is shown in Fig. 10. The resolution is clearly increasing with P_B in both detectors. Centrally produced B's have relatively modest momenta with only a small fraction in the tail above 20 GeV, while the mean momentum of forwardly produced B's is ~ 50 GeV. For a given P_B, the proper time resolution of the detectors is remarkably similar, within about 10% of each other. The better resolution of the forward detector is simply a consequence of the higher momentum of the

B decays within its acceptance.

We are also interested in the effect of final state multiplicity on the significance of separation. The decays $B_d^0 \to \pi^+\pi^-$ and $B_s^0 \to D_s^-\pi^+\pi^+\pi^-$ have different multiplicity than $B_d^0 \to J/\psi\, K_s$. Using a larger number of tracks to determine a vertex improves the error matrix. On the other hand, the lower p_T of each particle from a high multiplicity decay degrades the individual track error matrices. For example, the pions from $B_d^0 \to \pi^+\pi^-$ have higher momentum in the B rest frame than the muons and pions from the $B_d^0 \to J/\psi\, K_s$. This leads to larger opening angles and less multiple scattering in the lab frame. In principle, both of these effects lead to a better $L/\delta L$.

The quantity $\langle L/\delta L\rangle$ versus η_B for $B_d^0 \to \pi^+\pi^-$ for the forward and central detectors at the Tevatron is shown in Fig. 11. The forward detector has better resolution than the central, as was the case with $B_d^0 \to J/\psi\, K_s$. Additionally, a comparison of $\langle L/\delta L\rangle$ for $B_d^0 \to J/\psi\, K_s$ (Fig. 6) and $B_d^0 \to \pi^+\pi^-$ (Fig. 11) shows that the shapes of the distributions are about the same but on average $\langle L/\delta L\rangle$ is slightly better for $B_d^0 \to \pi^+\pi^-$ for both detectors.

For $B_s^0 \to D_s^-\pi^+\pi^+\pi^-$ the value of $\langle L/\delta L\rangle$ as a function of η_B for the two detectors is also shown in Fig. 11. These distributions are similar to the distributions for $B_d^0 \to J/\psi\, K_s$ and $B_d^0 \to \pi^+\pi^-$. The forward detector, once again, has better $\langle L/\delta L\rangle$.

The results above show that the significance of separations are comparable for the three decay modes. The various effects of multiplicity cancel so that $L/\delta L$ is roughly independent of multiplicity.

D. Mass Resolution

A narrow mass peak serves at least two important purposes: it improves the signal to background ratio and allows for separation of reflection peaks due to particle misidentification. An example of the latter is when $B_d^0 \to K^+\pi^-$ or $B_s^0 \to K^-\pi^+$ is misidentified as $B_d^0 \to \pi^+\pi^-$. Mass resolution is calculated from the track error matrices. A comparison of the central and forward detectors' mass resolution for the J/ψ from $B_d^0 \to J/\psi\, K_s$ at the

Tevatron is shown in Fig. 12. The mass resolutions are similar for both detectors, about 10 MeV. For both detectors, the mass resolution degrades at higher values of η_B. In the central detector, this degradation is caused by tracks at high η exiting the detector before reaching the outer radius. In the forward detector, the degradation of the mass resolution is caused by the increased momentum of the B_d^0.

We also studied the mass resolution of the B for the decays $B_d^0 \to \pi^+\pi^-$ and $B_s^0 \to D_s^-\pi^+\pi^+\pi^-$. We expect the resolution from $B_d^0 \to \pi^+\pi^-$ to be worse due to the greater available energy in this decay. The mass resolutions of the B_d^0 and B_s^0 versus η_B are shown in Fig. 13. The mass resolution for both detectors is about the same, approximately 20 MeV for the B_d^0 and 10 MeV for the B_s^0. There is a degradation at high η_B in both detectors. The shapes are similar to those for the J/ψ but degrade more rapidly with η_B in both detectors.

Although the mass resolution of both detectors considered here is very similar, this does not imply that all forward and central detectors will have the same mass resolution. The mass resolution is a strong function of the momentum resolution. For both the forward and central detector, the momentum resolution is dependant on the measurement length. A central detector with a smaller tracking radius or a forward detector shorter than those of the fixed target experiments we used to parameterize the momentum resolution would have worse momentum resolution.

E. Vertex Detector Optimization

The designs of the detectors presented above are motivated by existing detectors and prototypes. To optimize detector performance, several critical detector parameters are examined. We studied the effect on $\langle L/\delta L \rangle$ of varying three of the vertex detector parameters: inner radius, detector resolution, and stereo angle. For these studies the parameters are varied individually and other parameters are held at their nominal values. These studies are performed using the $B_d^0 \to J/\psi\, K_s$ decay mode at the Tevatron.

1. Inner Radius

Reducing the inner radius, R_{min}, of a vertex detector improves the vertex resolution. This is due to the decreased distance that a track must be extrapolated from the closest measurement to the vertex. Despite this advantage, a smaller radius detector is generally more difficult to build and suffers more radiation damage. Thus, it is of interest to determine how much the vertex resolution improves with decreasing inner radius.

Since the nominal value of R_{min} of the forward detector is 0.5 cm and of the central detector is 3.0 cm, radii in this range are examined. The values of $\langle L/\delta L \rangle$ for the central detector at the Tevatron are presented in Table ?? over the range studied. There is a factor of about two improvement in $\langle L/\delta L \rangle$ for a factor of six reduction in inner radius. There is little improvement in $\langle L/\delta L \rangle$ for $R_{min} < 1$ cm. This illustrates that at a sufficiently small inner radius the error due to extrapolation distance can be less than that due to detector resolution.

For the forward detector, $\langle L/\delta L \rangle$ is also presented in Table ??. The values of R_{min} used are the same as above. There is a factor of more than 4 improvement in $\langle L/\delta L \rangle$ over this range of radii. Some of the improvement in Table ?? is due to the increase in the number of planes traversed by each track with the decrease in inner radius. This has two effects which reduce the error in the track parameters: a greater the number of measurements are made on each track and more tracks at higher η are accepted.

2. Detector Resolution

The current CDF detector has strips that measure in the $r - \phi$ direction; the addition of stereo strips allows for three dimensional measurements of vertices. These stereo strips are usually at small angle or at 90° (z-strips). The problem with z-strips is that it is difficult to route the signals to the end caps of a cylindrical detector. For this reason, a coarser resolution of z-strips, and therefore fewer channels, is advantageous if it does not degrade

the vertex resolution significantly. Therefore, the resolutions of the $r-\phi$ and z-strips should not necessarily be the same.

For this study, the $r-\phi$ resolution is held constant at the nominal value, 13μm, and the z-strip resolution is varied from 5 to 500 μm. The values of $\langle L/\delta L \rangle$ for various z-strip resolutions at the Tevatron are shown in Table ??. The factor of 100 variation in resolution yields a factor of about 3.5 in $\langle L/\delta L \rangle$. There is little improvement in $\langle L/\delta L \rangle$ for z-strip resolution of less than 50 μm.

Particles in a forward detector have a higher average momentum than those in a central detector. Therefore, improving the detector resolution is more likely to improve the track error matrices and thus $\langle L/\delta L \rangle$. However, improvements in resolution are difficult and expensive, both in development and construction. Therefore, we want to find the maximum acceptable resolution.

For the forward detector, the x and y resolutions are varied together from 5 to 30 μm. The values of $\langle L/\delta L \rangle$ for these resolutions are presented in Table ??. There is a factor of 2 improvement in $\langle L/\delta L \rangle$ for the factor of 6 improvement in resolution. There is only modest improvement in $\langle L/\delta L \rangle$ from reducing the resolution below 10 μm.

3. Stereo Angle

For a central detector, a larger stereo angle gives better z resolution for the same strip resolution. Large angle stereo, however, is more difficult to implement, as discussed above.

The values of $\langle L/\delta L \rangle$ for a range of stereo angles from 5° to 90° are shown in Table ??. There is a factor of 2 improvement from varying the stereo angle from 5° to 90°. Little improvement, however, is seen for stereo angles larger than 20°. We also studied reducing the resolution of the 5° stereo strips from 30μm to 13μm. This yields only a 25% improvement in the mean significance of separation. Also, little improvement is seen for 5° strips compared to having no strips. This is because the small stereo angle does not significantly improve the z resolution beyond that attained with the VTPC.

IV. SUMMARY AND CONCLUSIONS

We examined the B-physics capabilities of two representative detector designs: a central detector based on the CDF detector, and a forward detector adapted from fixed target charm experiments. We studied acceptance, decay time resolution, and mass resolution, for B-production at three colliders: RHIC, the Tevatron, and LHC. We find that comparable mass resolutions for B-decays are achievable in the forward and central detectors, and that the forward detector has much better proper time resolution, at all three colliders. At RHIC, a central detector accepts a much larger fraction of B-decays than a forward detector (a factor of 6 for our models), giving it a decided advantage in physics potential. At the Tevatron and LHC, the acceptances are comparable.

We find that for the central detector, for inner radii of less than 1 cm, there is little additional improvement in decay time resolution. We also find that measurement resolutions better than about $10\,\mu$m do not significantly improve decay time resolution for either the forward or central detector with the nominal inner radii used in this study.

The analytic method used in this analysis provides a quick and accurate assessment of performance for a variety of detector geometries and a wide range of physics processes and detector parameters.

ACKNOWLEDGEMENTS

The authors express their thanks to Alan Sill and Walter Innis for providing the track error matrix code for a solenoidal detector. This code was useful in early analyses. We also thank Paul Avery for his notes on the mathematical aspects of particle track and vertex fitting. For useful discussion, we thank Walter Selove and other colleagues working toward dedicated beauty experiments at FNAL and BNL. Finally, we thank the Texas National Research Laboratory Commission and the U.S. Department of Energy for financial support.

REFERENCES

[1] Y. Nir and H. R. Quinn, Annu. Rev. Nucl. Part. Sci. **42**, 211 (1992).

[2] I. Dunietz, in *Proceedings of the Workshop on B Physics at Hadron Accelerators, Snowmass, Colorado*, 1993, edited by P. McBride and C. S. Mishra, p. 83.

[3] R. Aleksan, B. Kayser, and P. Sphicas, in *Proceedings of the Workshop on B Physics at Hadron Accelerators, Snowmass, Colorado*, 1993, edited by P. McBride and C. S. Mishra, p. 291.

[4] R. Edelstein et al., "Expression of Interest for a Dedicated Hadron Collider B Experiment at the Fermilab Tevatron", 1994.

[5] H. Bengtsson and T. Sjostrand, Comp. Phys. Comm. **46**, 43 (1987); T. Sjostrand and M. Bengtsson, Comp. Phys. Comm. **43**, 367 (1987).

[6] P. Billoir, R. Fruhwirth, and M. Regler, Nucl. Instrum. Methods **A241**, 115 (1985).

[7] R. F. Harr, submitted to Nucl. Instrum. Methods.

[8] C. J. Kennedy, R. F. Harr, and P. E. Karchin, in *Proceedings of the Workshop on B Physics at Hadron Accelerators, Snowmass, Colorado*, 1993, edited by P. McBride and C. S. Mishra, p. 707.

[9] F. Abe *et al.*, Phys. Rev. Lett. **72**, 3456 (1994).

[10] E. L. Berger and R. Meng, Phys. Rev. D **46**, 169 (1992).

[11] F. Abe et al., Nucl. Instrum. Methods **A271**, 387 (1988).

[12] J. D. Lewis, J. Mueller, J. Spalding, and P. Wilson, in *Proceedings of the Workshop on B Physics at Hadron Accelerators, Snowmass, Colorado*, 1993, edited by P. McBride and C. S. Mishra, p. 217.

[13] R. L. Gluckstern, Nucl. Instrum. Methods **24**, 381 (1963).

[14] F. Abe *et al.*, Phys. Rev. Lett. **71**, 3421 (1993).

[15] P. L. Frabetti et al., Nucl. Instrum. Methods **A320**, 519 (1992).

[16] J. Ellett et al., Nucl. Instrum. Methods **A317**, 28 (1992).

TABLE I. Characteristics of the 3 hadron colliders considered for a future B-physics experiment. The production cross sections are taken from Berger and Meng [9].

Collider	energy (TeV)	beam particles	B cross section (μbarn)
RHIC	0.5	pp	7 - 8
Tevatron	1.8	$p\bar{p}$	40 - 50
LHC	14.0	pp	200 - 500

TABLE II. Design parameters for the central and forward detector models. Each layer in the central detector is a cylindrical surface of the listed radius. In the forward detector, the beampipe is a cylindrical surface and the silicon detectors are planes normal to $\hat{z}$.

	detector layer		scattering		measurement	
name	location		thickness	rad. len.	direction	resolution
	r (cm)	z (cm)	(cm)	(%)		(μm)
		Central Detector				
beampipe	2.5	-	0.1	0.28	-	-
SVX	3.0, 4.0, 5.5, 8.0	$-50 < z < 50$	0.03	0.32	r-z	30
					r-ϕ	13
VTPC	9.0	$-80 < z < 80$	0.1	0.53	-	-
	16 layers from 10 to 21 cm	$-80 < z < 80$	0.75	0.002	r-z	200
	22.0	$-80 < z < 80$	0.2	1.1	-	-
CTC	27.7	$-160 < z < 160$	0.2	1.1	-	-
	84 layers from 30 to 131	$-160 < z < 160$	1.2	0.004	$\perp$ to wire	200
		Forward Detector				
beampipe	0.5	-	0.03	0.08	-	-
silicon	$0.5 < r < 10$	10 planes from 2 to 38 cm	0.03	0.32	x-z	10
					y-z	10

TABLE III. Percentage of accepted events for tagged $B_d^0 \to \pi^+\pi^-$, $B_d^0 \to J/\psi\, K_s$, and $B_s^0 \to D_s^-\pi^+\pi^+\pi^-$.

Decay	RHIC	Tevatron	LHC
$B_d^0 \to \pi^+\pi^-$			
Forward	0.7	1.9	3.2
Central	6.7	4.2	3.3
$B_d^0 \to J/\psi\, K_s$			
Forward	0.6	1.7	2.7
Central	3.6	2.4	1.7
$B_s^0 \to D_s^-\pi^+\pi^+\pi^-$			
Forward	0.4	1.2	2.3
Central	1.7	1.1	1.1

TABLE IV. Mean significance of separation for $B_s^0 \to J/\psi K_s$ for various inner radii at the Tevatron.

Inner Radius (mm)	Central Detector	Forward Detector
5	25	57
10	23	42
20	17	21
30	12	14

TABLE V. Mean significance of separation for $B_s^0 \to J/\psi K_s$ for various resolutions at the Tevatron. For the central detector the resolution of the r-ϕ strips is held at 13 μm and the resolution of the z strips is varied.

Resolution (μm)	Significance of Separation
Central	
5	15.0
30	12.3
50	10.5
100	8.5
250	5.7
500	4.4
Forward	
5	68
10	57
20	41
30	32

TABLE VI. Mean Significance of separation for $B_s^0 \to J/\psi K_s$ for various stereo angles and resolution of stereo strips for the central detector at the Tevatron.

Stereo Angle	Resolution (μm)	Significance of Separation
90°	30	12.3
45°	30	11.7
20°	30	9.3
5°	30	5.5
5°	13	6.4
none		4.5

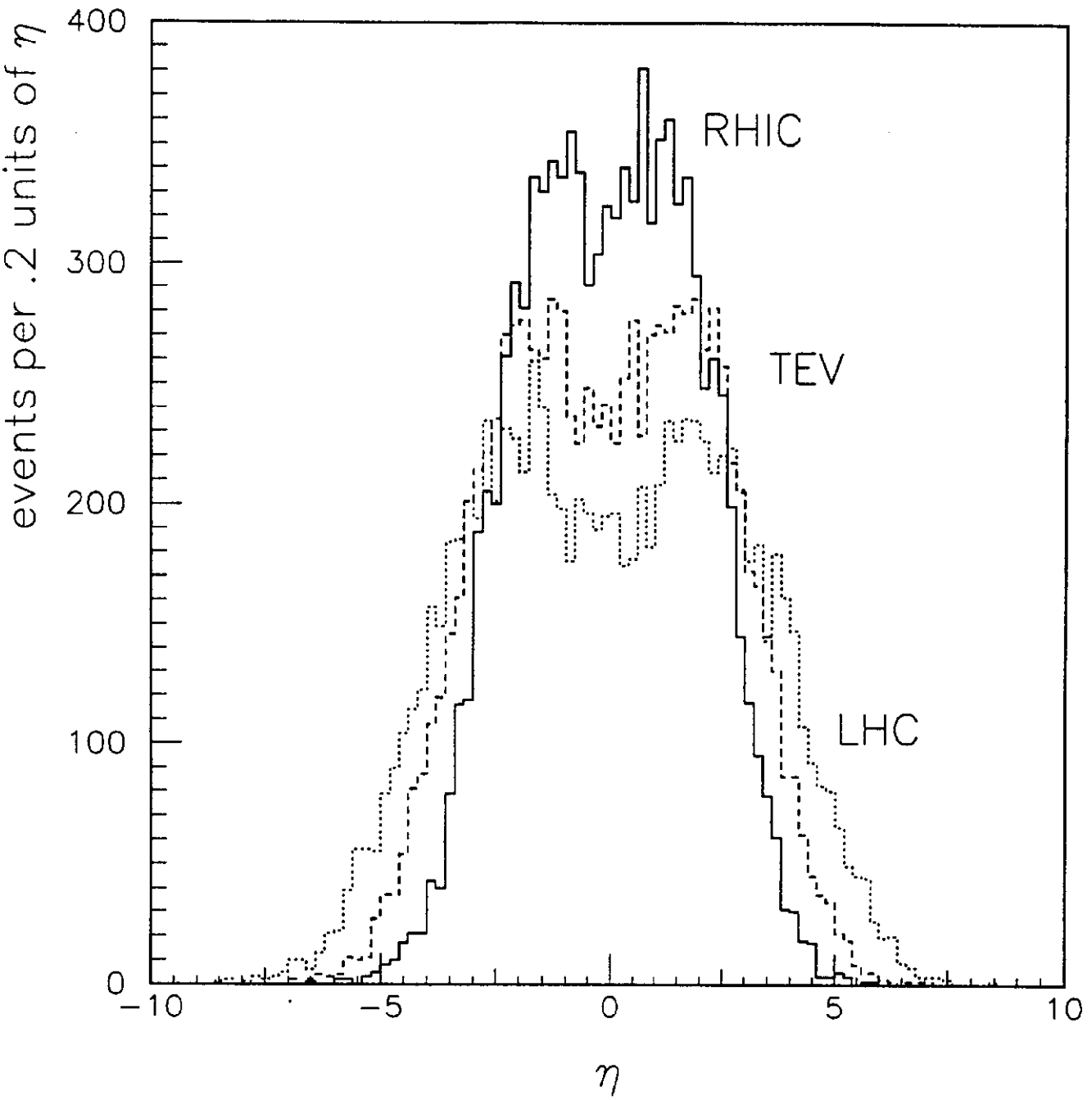

FIG. 1. Distribution in pseudo-rapidity (η) for B_d^0 at RHIC (solid), the Tevatron (dashed), and LHC (dotted), as predicted by PYTHIA. Each histogram contains 10,000 entries.

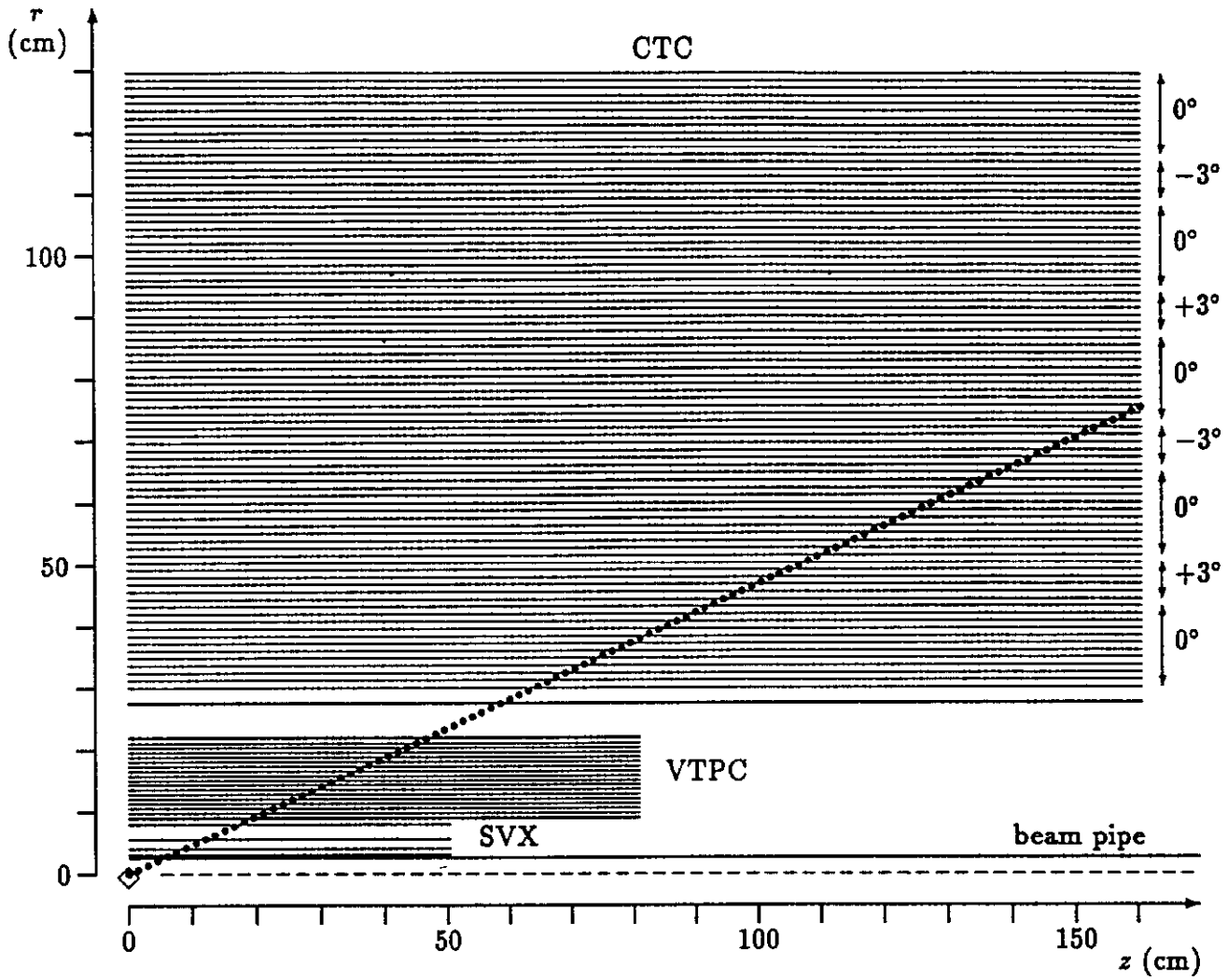

FIG. 2. One quadrant of an r-z cutaway view of the central detector model. The interaction point and beam line are represented by the diamond and dashed line, respectively. All the elements used in the calculation are represented: the beam pipe, the 4 SVX layers; the inner shell, 16 measuring layers, and outer shell of the VTPC; and the inner shell and 84 measuring layers of the CTC. The pattern of stereo wires in the CTC is labeled along the right edge. The dotted line is drawn at $\eta = 1.5$, the acceptance limit of the detector. The entire detector is immersed in a 1.5 T solenoidal magnetic field.

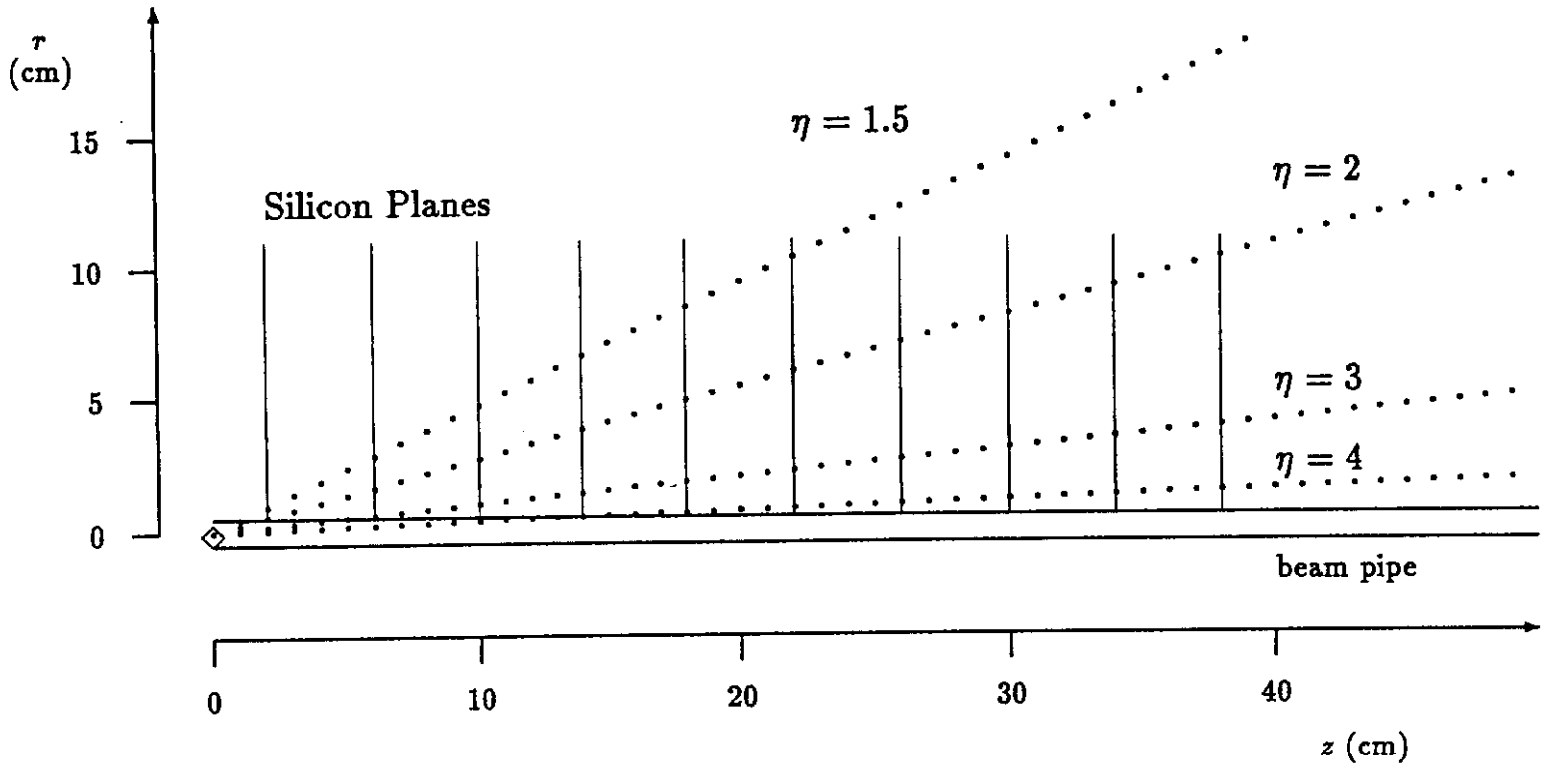

FIG. 3. The forward vertex detector model viewed in r-z. The interaction point is represented by the diamond. There are 10 planes of double sided silicon detectors spaced every 4 cm from 2 to 38 cm downstream of the interaction point.

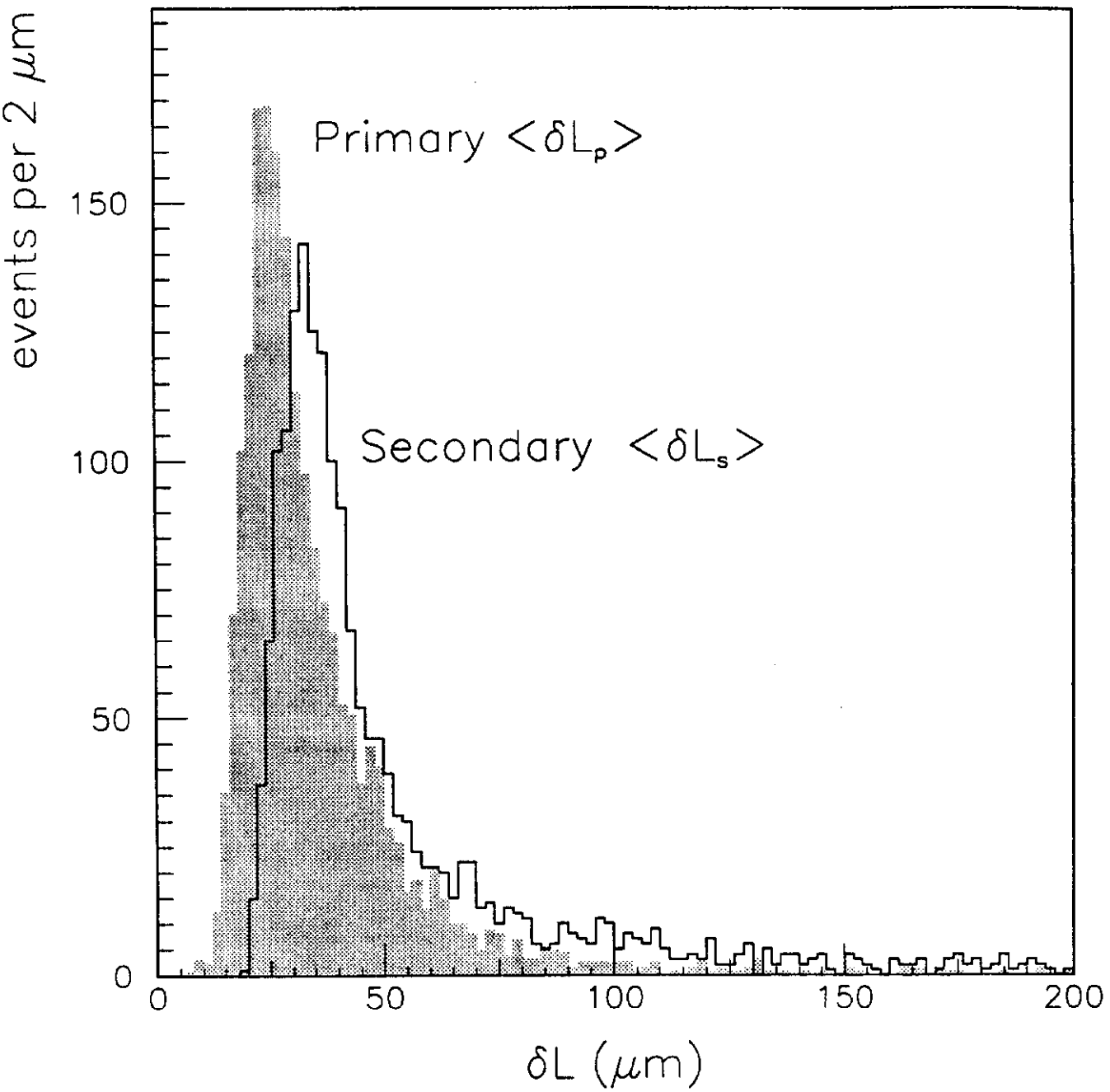

FIG. 4. Distributions of resolutions of the primary and secondary vertices in the direction of the decaying B particle for the central detector model at the Tevatron. The secondary vertex resolution is determined by vertexing muons from $B_d^0 \to J/\psi\, K_s$, $J/\psi \to \mu^+\mu^-$.

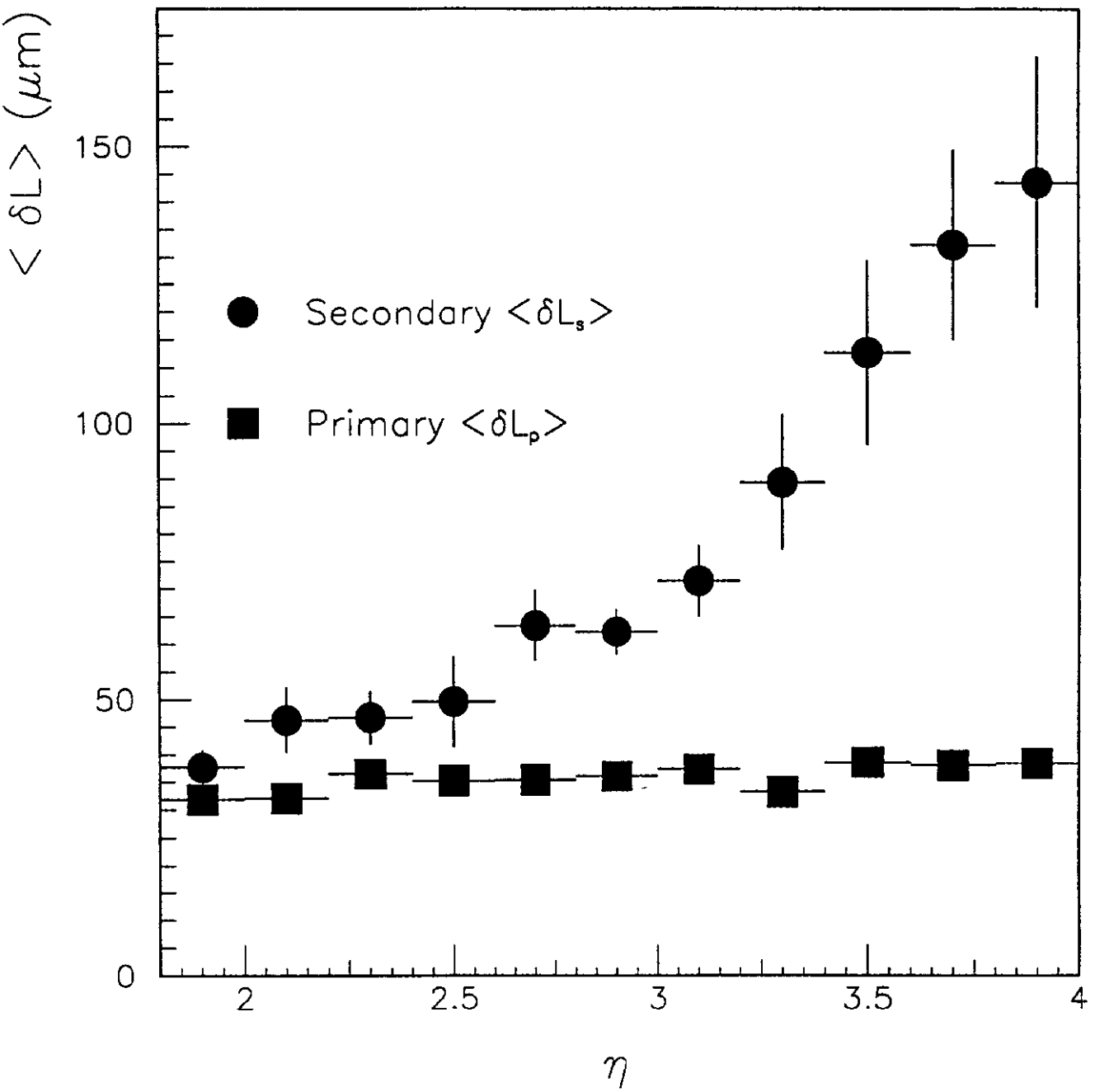

FIG. 5. Mean resolution on the position of the primary and secondary vertices in the direction of the decaying B particle versus η_B for the forward detector model at the Tevatron. The secondary vertex resolution is determined by vertexing muons from $B_d^0 \to J/\psi K_s$, $J/\psi \to \mu^+\mu^-$.

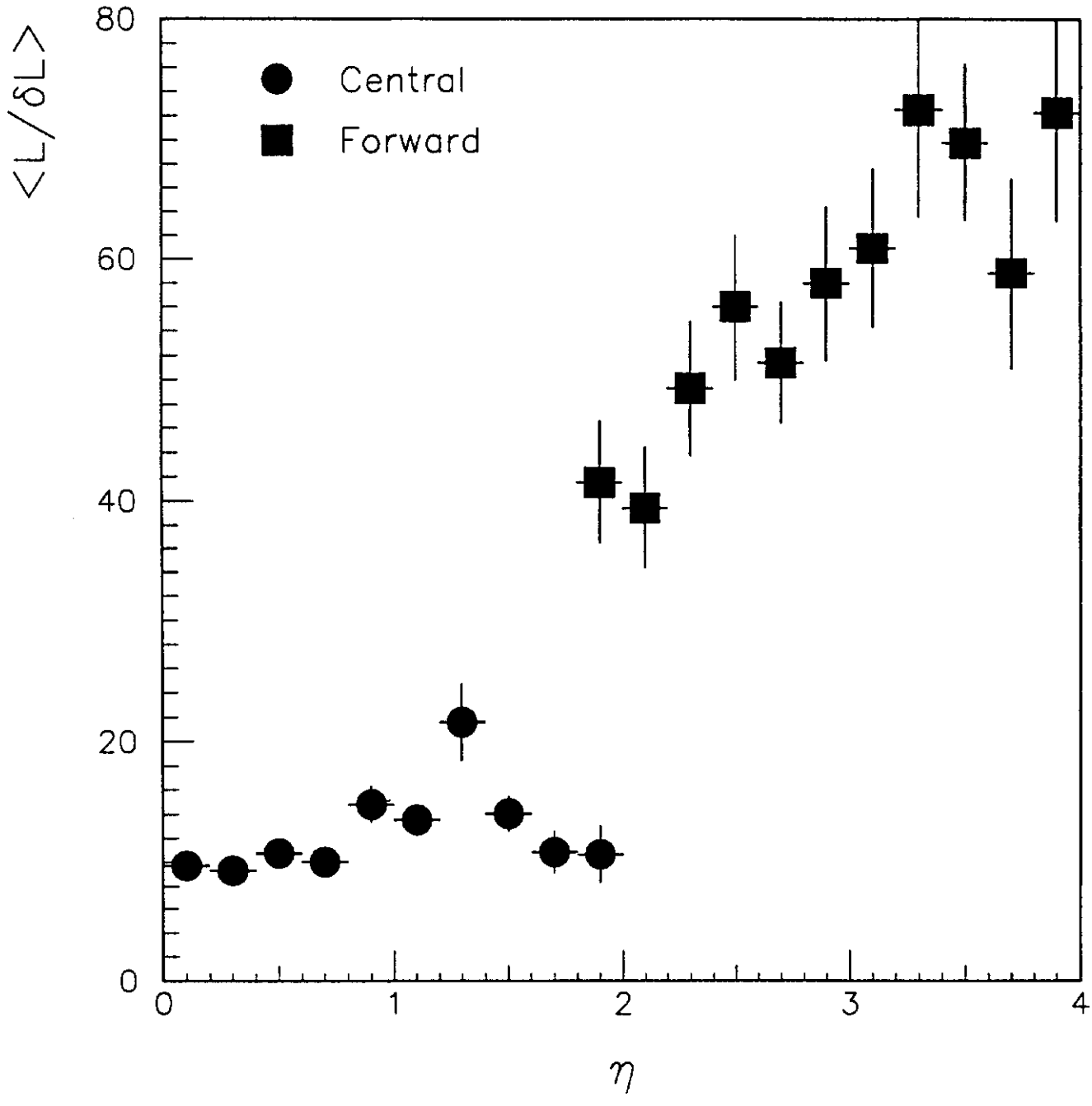

FIG. 6. $\langle L/\delta L \rangle$ versus η_B for $B_d^0 \to J/\psi K_s$ at the Tevatron.

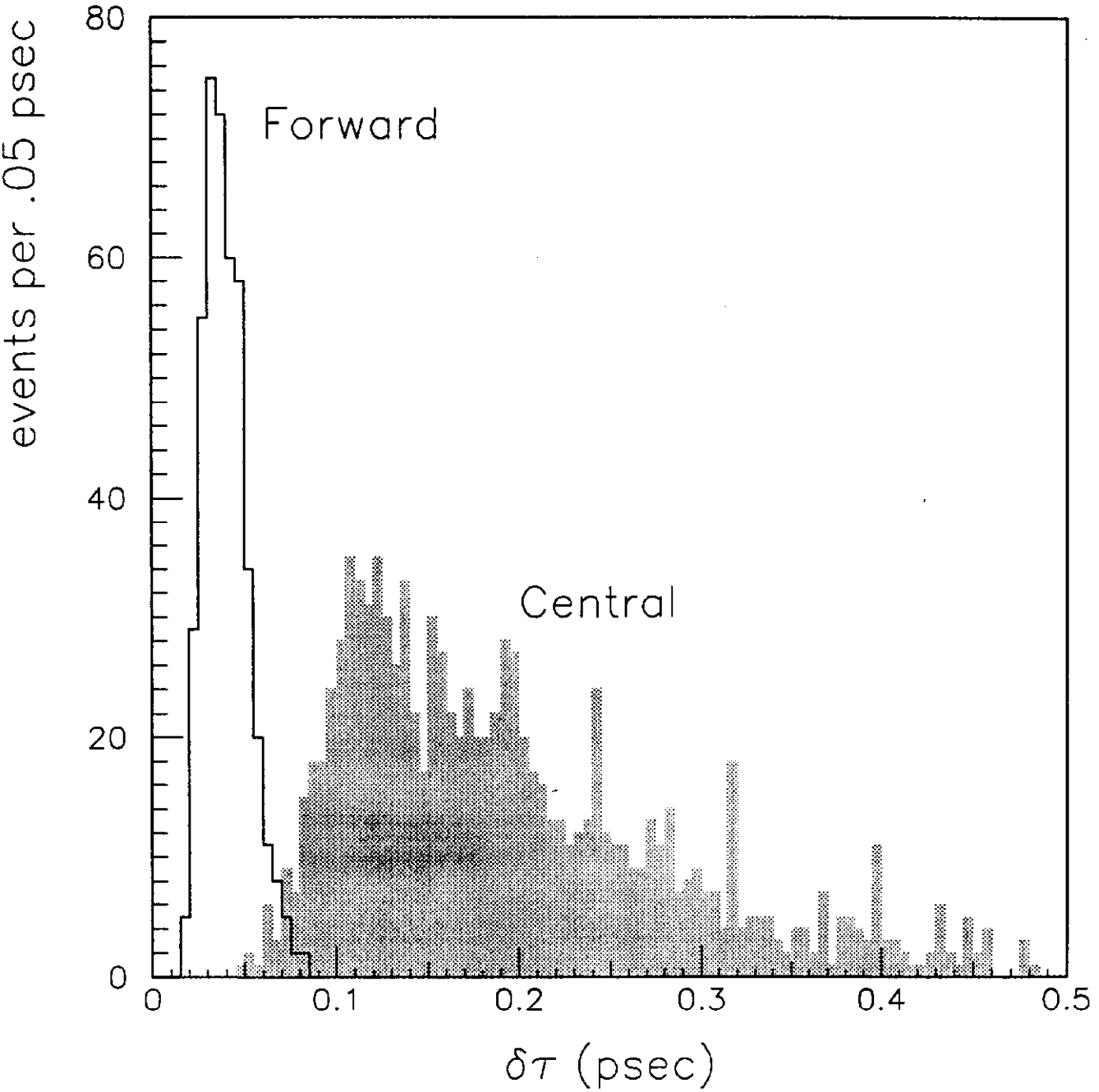

FIG. 7. $\delta\tau$ distribution of accepted $B_s^0 \to D_s^- \pi^+ \pi^+ \pi^-$ decays at RHIC for the central (shaded) and forward (unshaded) detector. This is an untagged sample. For the tagged sample the acceptance advantage in the central detector is an additional factor of two greater.

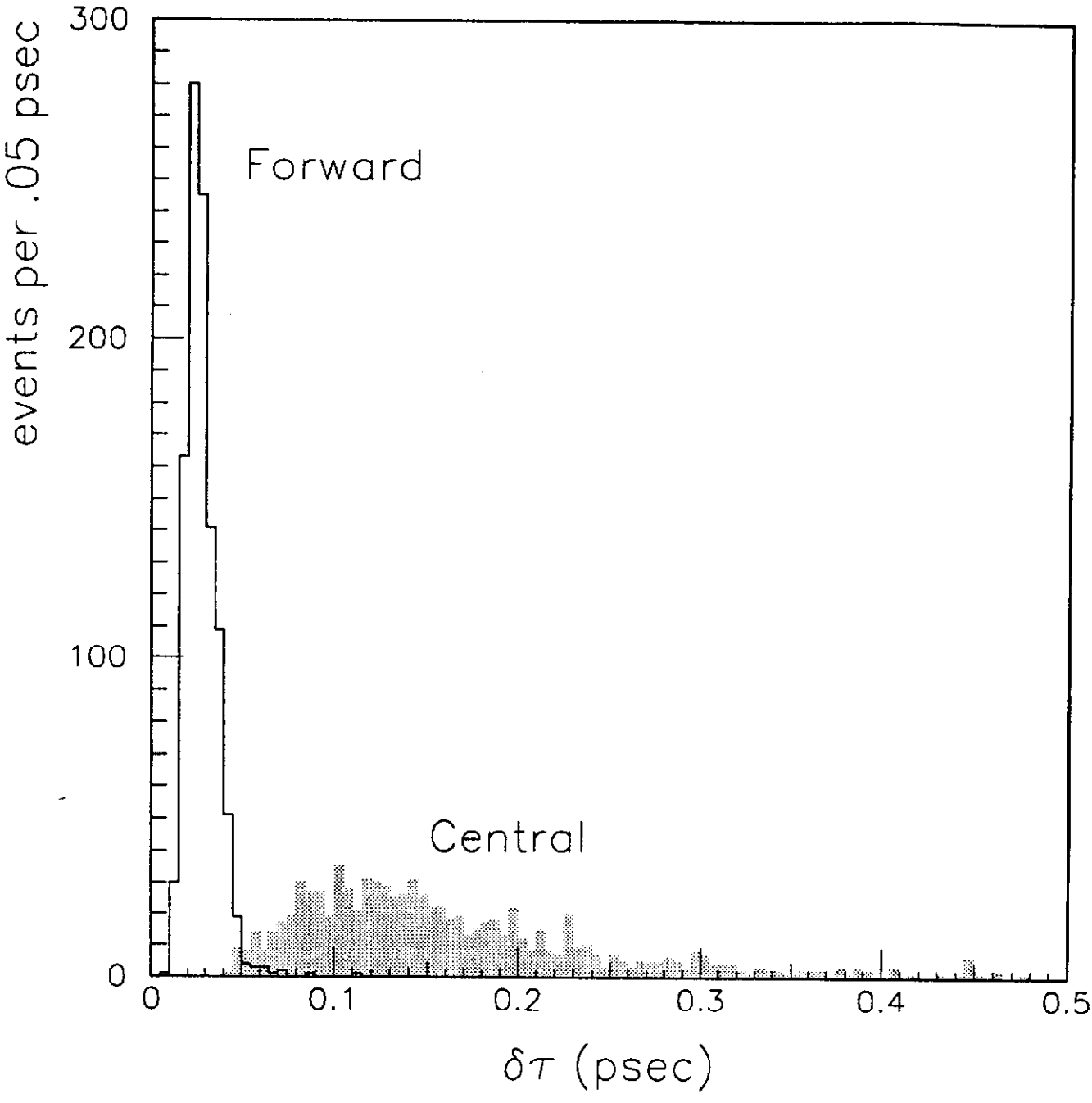

FIG. 8. Same as Fig. 7 except at the Tevatron. The relative acceptances between the forward and central detectors for the tagged and untagged samples are about the same.

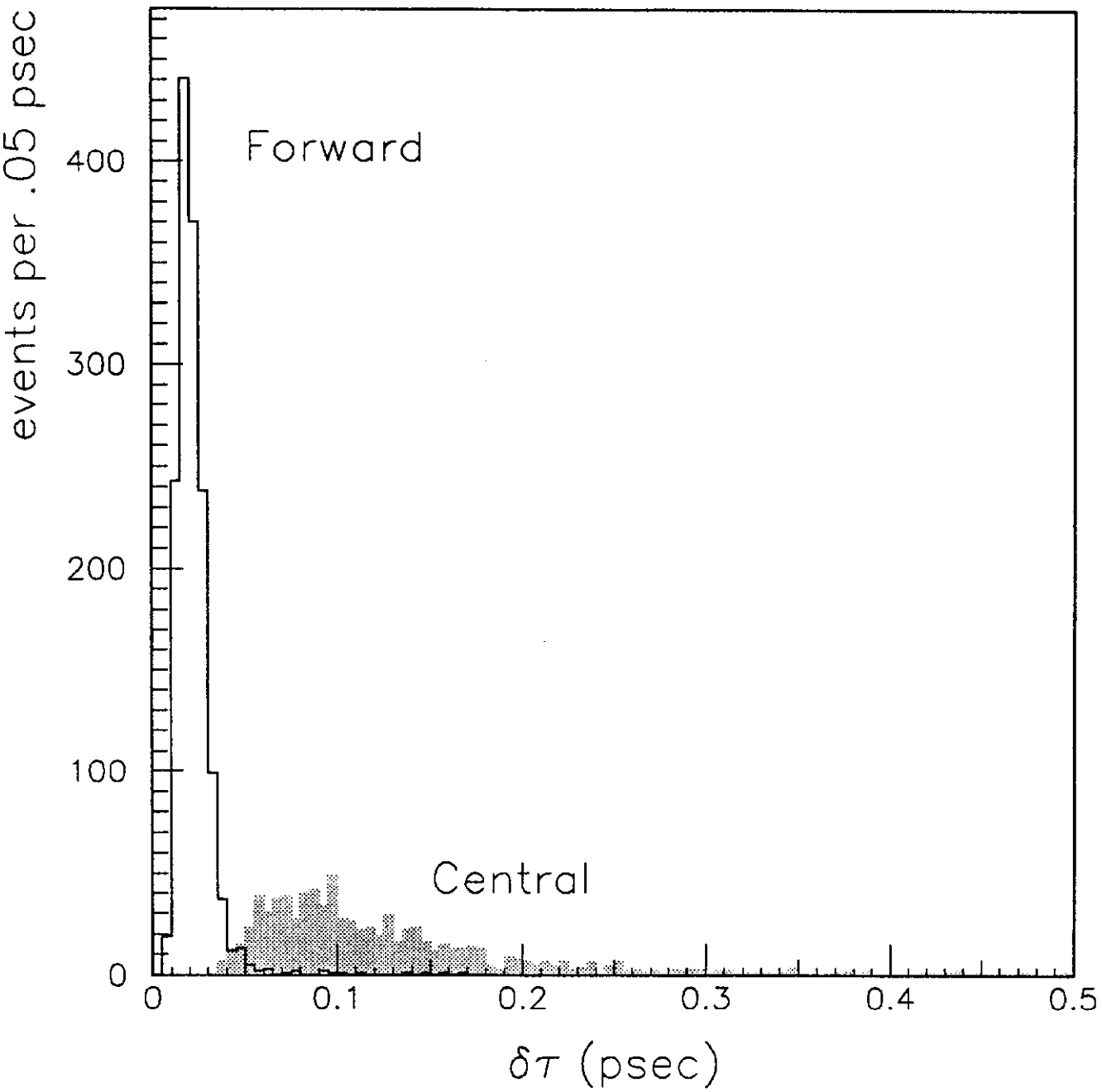

FIG. 9. Same as Fig. 7 except at LHC. The relative acceptances between the forward and central detectors for the tagged and untagged samples are about the same.

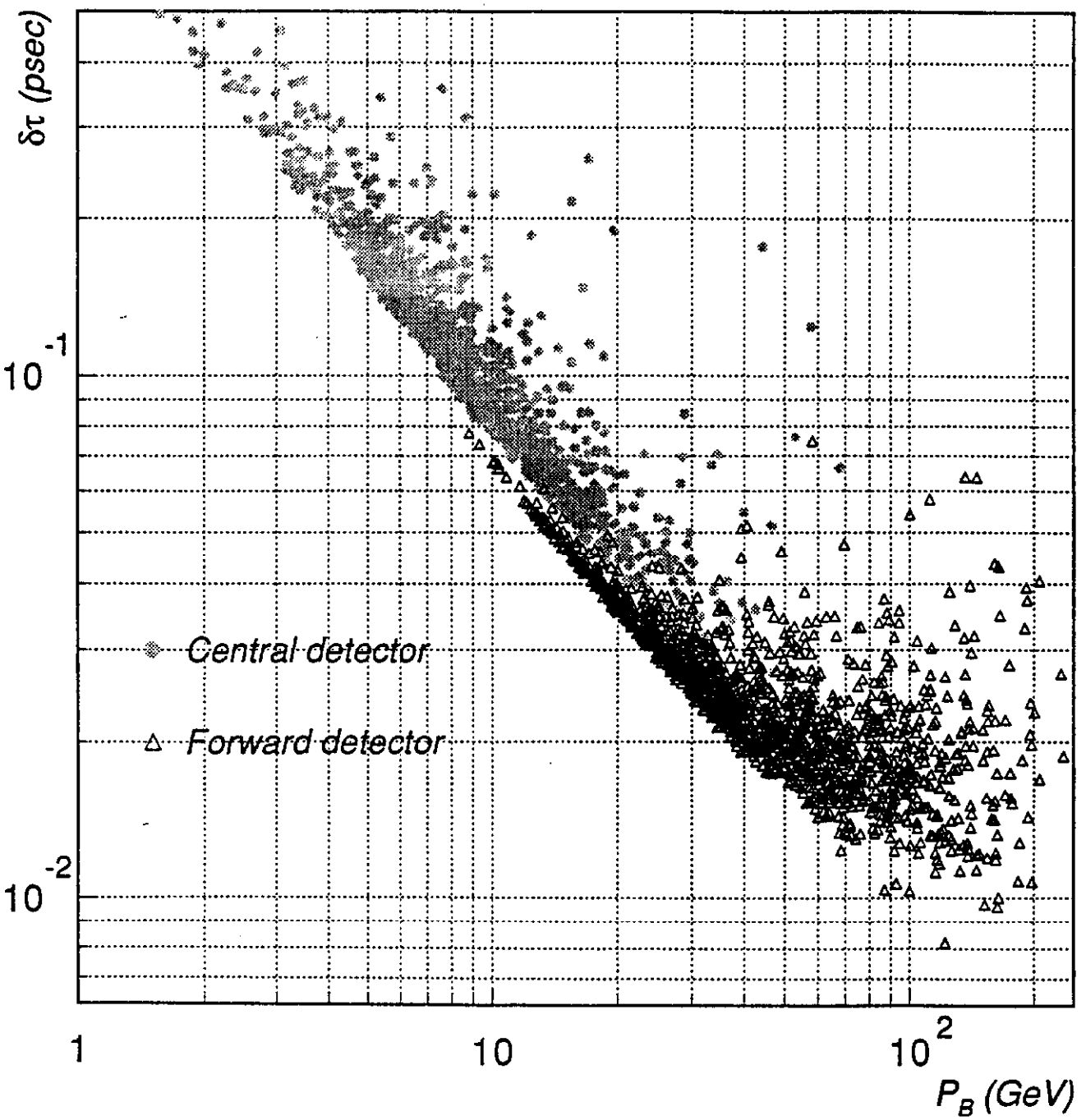

FIG. 10. Proper time resolution versus the momentum of the reconstructed $B_s^0 \to D_s^- \pi^+ \pi^+ \pi^-$ at the Tevatron. In the region where the two distributions overlap, only a few of the central detector points are obscured by the forward detector points. Notice that for a given B momentum, the resolution of the detectors is nearly the same. However, due to the strong correlation, the forward detector, which accepts B decays of higher momentum, achieves better overall proper time resolution.

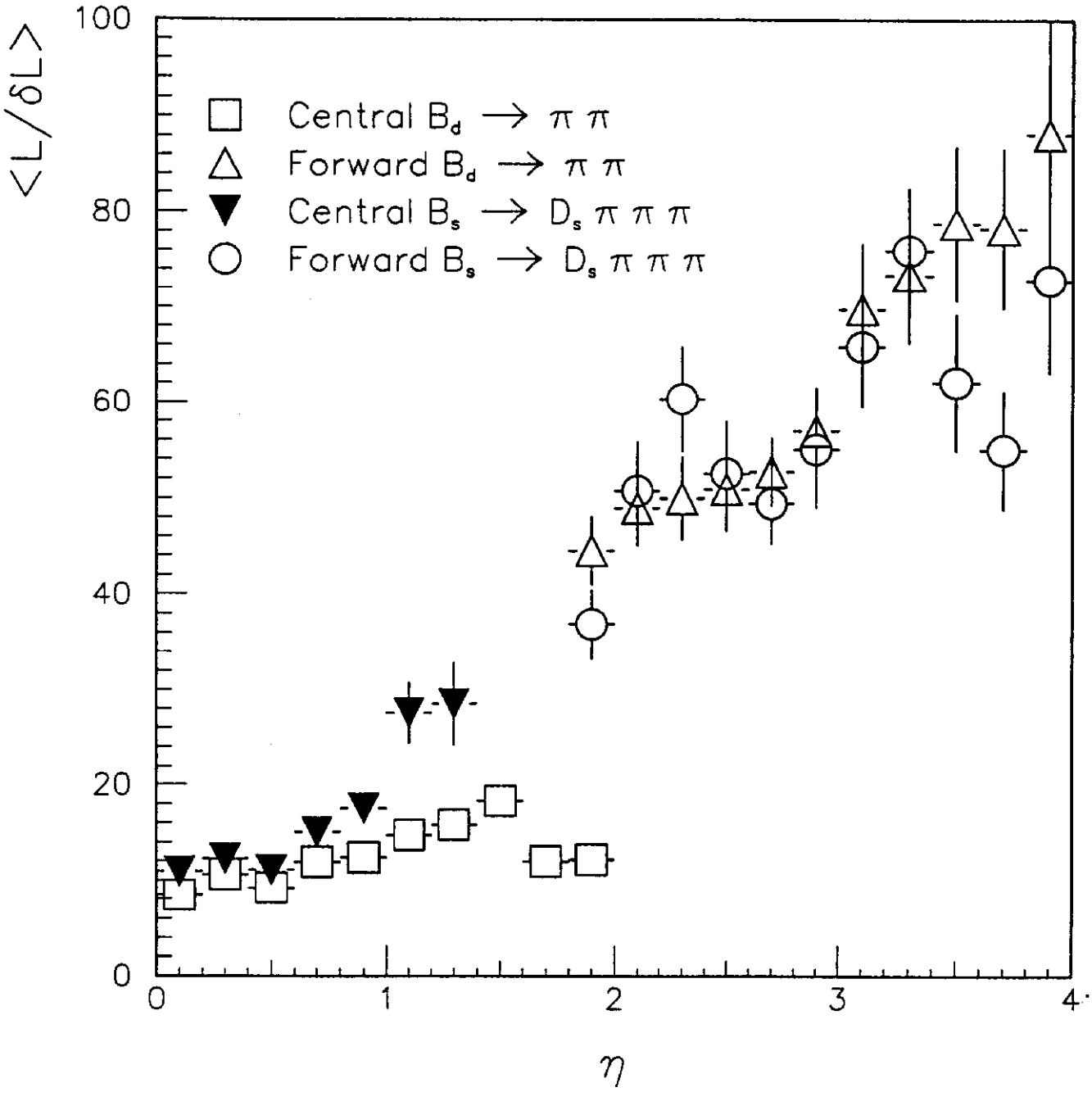

FIG. 11. Same as Fig. 6 except for decays $B_d^0 \to \pi^+\pi^-$ and $B_s^0 \to D_s^-\pi^+\pi^+\pi^-$.

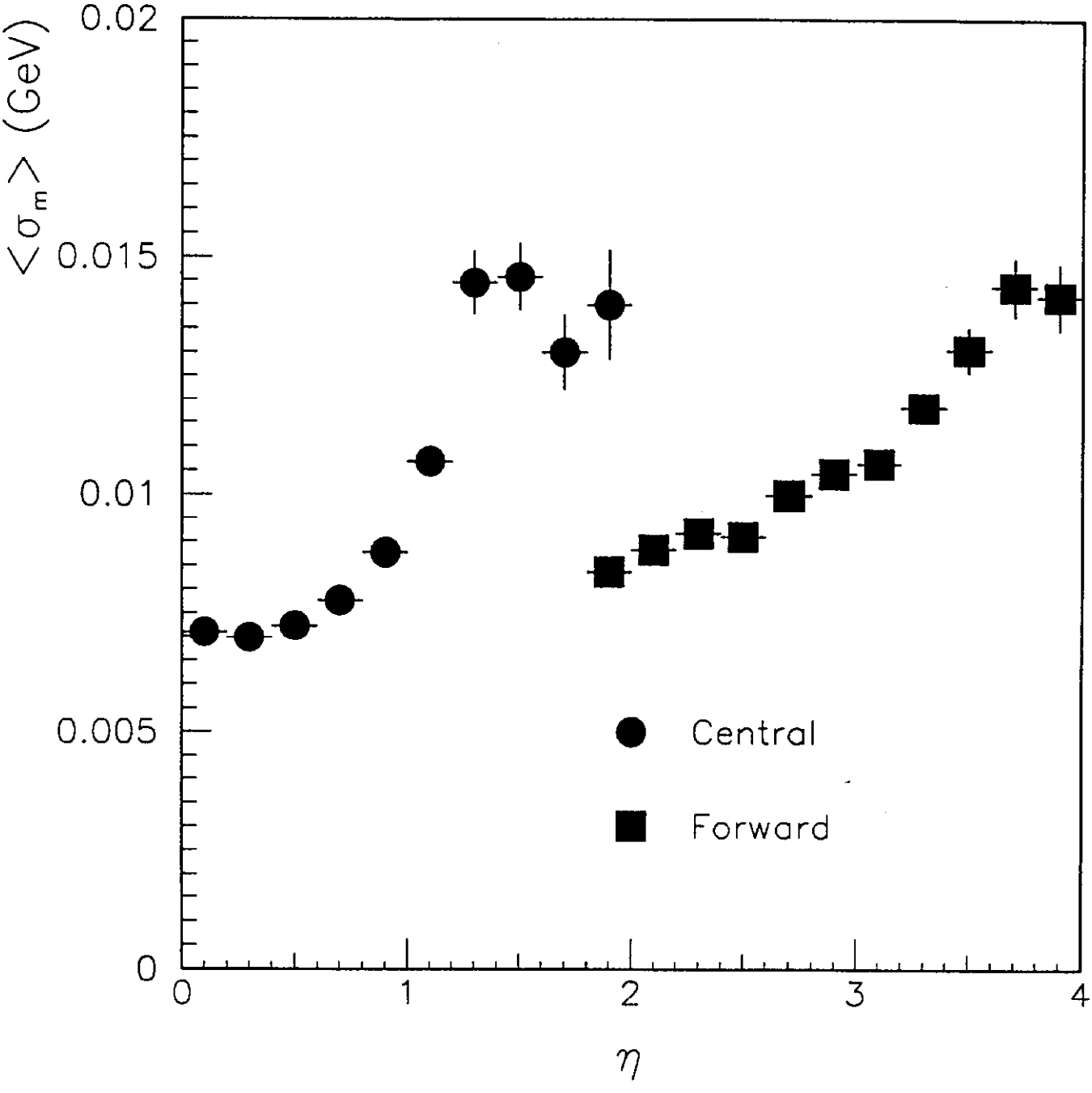

FIG. 12. $\langle \sigma_m \rangle$ of the J/ψ vs η_B for the decay $B_d^0 \rightarrow J/\psi K_s$ at the Tevatron.

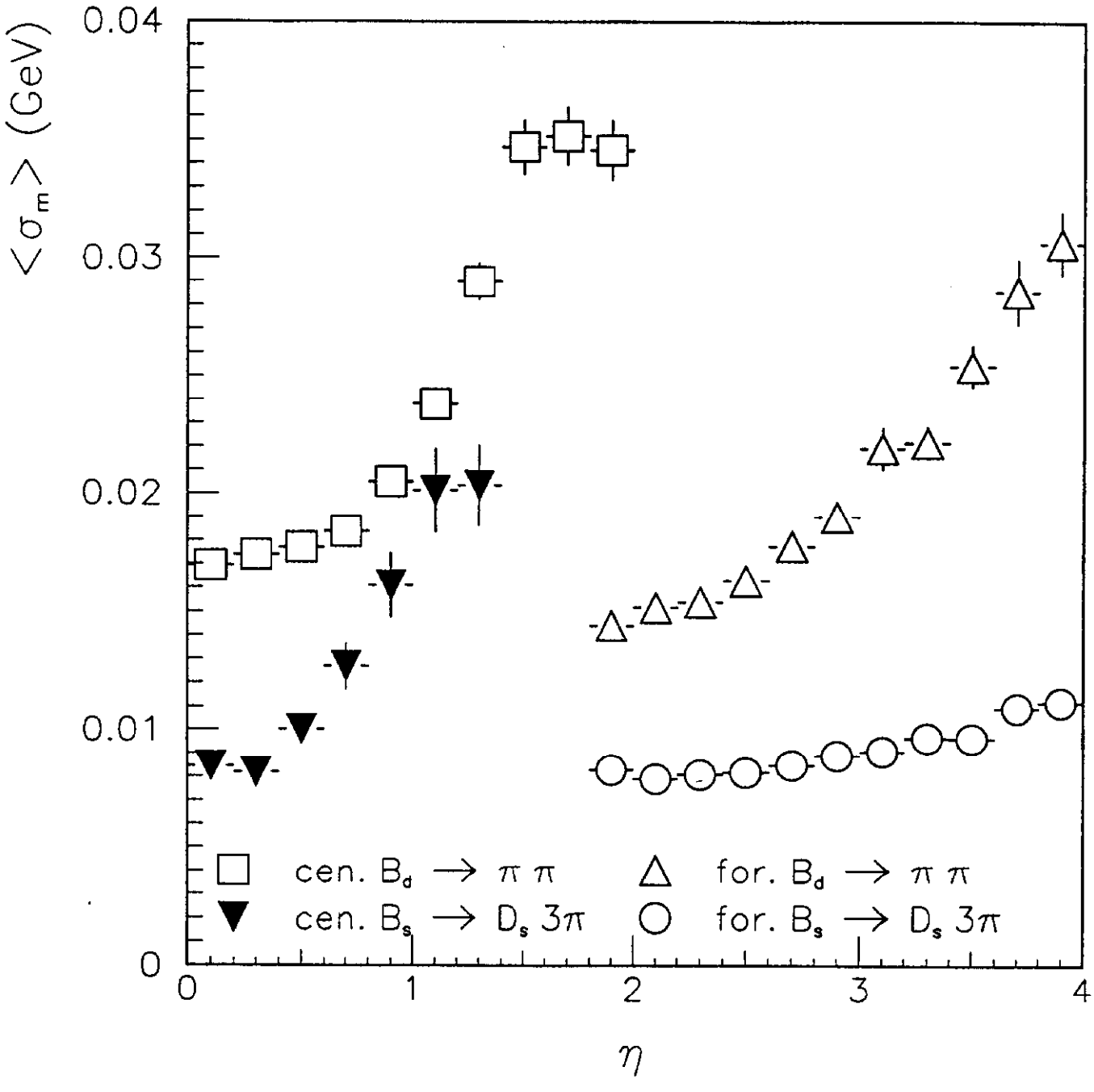

FIG. 13. $\langle\sigma_m\rangle$ of the B_d^0 and B_s^0 vs η_B for the decays $B_d^0 \to \pi^+\pi^-$ and $B_s^0 \to D_s^-\pi^+\pi^+\pi^-$ at the Tevatron.